

# Self-similar collapse of collisional gas in an expanding Universe

Leonid Chuzhoy and Adi Nusser

*Physics Department, Technion, Haifa 32000, Israel*

*E-mail: cleonid@tx.technion.ac.il, adi@physics.technion.ac.il*

27 October 2018

## ABSTRACT

Similarity solutions are found for the adiabatic collapse of density perturbations  $\delta M/M \propto r^{-s}$  ( $s > 0$ ) in a flat universe containing collisional gas only. The solutions are obtained for planar, cylindrical, and spherical perturbations with zero initial pressure. For adiabatic index  $\gamma \geq 4/3$ , a shock develops at a fixed fraction of the current turnaround distance. Near the center of a spherical perturbations with  $\gamma > 4/3$  and  $s > 1/2$ , the gas is in quasi-hydrostatic equilibrium (pressure supported) and has an asymptotic power law density profile,  $\rho \sim r^{-3s/(s+1)}$ , independent of  $\gamma$ . For  $s \leq 1/2$ , the profile depends on  $\gamma$ , the pressure is finite, the temperature decreases inward, and gravity dominates pressure causing a continuous inward flow. Although for  $1/2 < s < 2$  the temperature decreases at the center, the gas is pressure supported. The pressure is finite in cylindrical perturbations for  $s \leq 2(\gamma - 1)/(3\gamma - 4)$ , and in planar perturbations for any  $s > 0$ . We also derive the asymptotic behaviour of the gas variables near the center in a universe dominated by collisionless matter. In such a universe, the gas in a spherical perturbation with  $s < 2$  cannot be pressure supported and the temperature approaches a constant near the center. The solutions and the asymptotic behaviour are relevant for modelling the gas distribution in galaxy clusters and pancake-like superclusters, and determining the structure of haloes of self-interacting dark matter with large interaction cross section.

**Key words:** cosmology: theory – gravitation – dark matter – baryons – intergalactic medium

## 1 INTRODUCTION

On scales larger than a few megaparsecs, pressure forces in the baryonic matter in the universe are negligible, so

arXiv:astro-ph/0005331v2 17 Jul 2000

the evolution of dark and baryonic matter is mainly determined by gravity. On small scales pressure becomes important and may segregate between the evolution of baryonic and dark matter. Pressure forces, cooling of gas, and star formation feedback, are key ingredients in galaxy formation. These ingredients combine to cause differences between the distributions of galaxies and dark matter (biasing), even on large scales where these effects are not directly important (e.g., Kaiser 1984, Dekel & Rees 1987, Kauffmann, Nusser & Steinmetz 1997, Benson et. al. 2000). On scales smaller than the Jeans length of the photo-heated intergalactic medium (IGM), pressure forces dominate gravity and can prevent the collapse of gas into dark haloes below a certain mass threshold. For haloes massive enough the temperature of the IGM can be neglected and the gas falls into the halo. The mean free path for collisions between gas particles inside a halo is  $\approx (200/\delta_c) (10^{-15}/\sigma) (1+z)^{-3} (0.1/\Omega_b h^2) 1.6\text{pc}$ , where  $\delta_c$  is the overdensity inside the virial radius and  $\sigma$  is a typical cross section for collisions in units of  $\text{cm}^2$ . This is smaller than the virial radius of a typical halo by a few orders of magnitude. Therefore, on its infall into the halo, the gas is likely to form shocks and transform its kinetic energy into heat. The hot dense gas can then cool to form stars which explode and inject energy into the halo gas. Detailed study of these processes under general conditions is not feasible. One can aim at a global parameterization based on general physical requirements which match observational data (Kauffman, White, Guiderdoni 1993, Somerville & Primack 1999, Cole et. al. 1994). Another route would be to study special aspects which can be treated by either numerical or analytical methods. Here we focus on the collapse of the baryonic gas in an Einstein-De Sitter universe, ignoring the gas initial temperature, cooling and heating processes. We assume that the collapse initiates from a symmetric scale free density peak, and that the velocity of each shell in the peak is taken to match the general expansion of the universe. The energy of each shell is negative and it will expand up to a maximum

distance before it starts falling towards the center of the perturbation. The maximum distance is termed the turnaround radius. Shell crossing is not allowed and the collapse can proceed in two distinct ways, either a shock wave forms, or shells accumulate at the center. Which of these possibilities actually occurs, depends on the physical conditions at the center. If the velocity vanishes at the center than a shock wave forms. If on the other hand physical conditions allow a non vanishing velocity at the center then the shells accumulate at the center (Bertschinger 1985). Inner boundary conditions can be arranged so that a shock is accompanied by the accumulation of central mass, but a proper stability analysis is needed to determine whether or not this is possible (Bertschinger 1985). In this paper we focus on shocked collapses without the formation of a central mass. Since the initial gas pressure is negligible, the collapse eventually develops in a self-similar way where the only relevant scale at any time is the radius of the shell at maximum expansion. Bertschinger (1985), and Forcada-Miro & White (1997) have studied similarity solutions in spherically symmetric perturbations with initial relative mass excess  $\delta M/M \propto r^{-3}$ , and  $r^{-2}$ , respectively. Here we derive similarity solutions in planar, cylindrical, and spherical geometries, for the collapse of a perturbation with  $\delta M/M \propto r^{-s}$  for any  $s > 0$  and adiabatic index  $\gamma \geq 4/3$ .

In section 2 we write the equations of motion for symmetric perturbations in planar, cylindrical, and spherical geometry. In section 3 we discuss the asymptotic behaviour of the fluid variables near the center, in the case of shocked collapse. In section 4 we present results of numerical integrations of the equations. In section 5 we derive asymptotic behaviour of the fluid variables in a universe dominated by collisionless dark matter. In section 6 we conclude with a discussion of the results and their potential astrophysical consequences.

## 2 THE EQUATIONS

We write the Newtonian equations of motion governing the adiabatic collapse of symmetric perturbations in a collisional fluid (gas) of adiabatic index  $\gamma$  and zero initial pressure. Except section 5, we restrict the analysis here and throughout to the collapse in a flat universe containing collisional gas only. The initial gas pressure is zero, so the expansion scale factor of the universe is  $a(t) \propto t^{2/3}$ , the Hubble function is  $H(t) = 2/(3t)$ , and the background density is  $\rho_c = 3H^2/(8\pi G) = 1/(6\pi Gt^2)$ .

Denote by  $r$  and  $v \equiv dr/dt$  the physical position and velocity of a gas shell, where  $r = 0$  is the symmetry center of the perturbation. Further, let  $\rho(r, t)$  and  $p(r, t)$  be the gas density and pressure at  $r$ . As in Fillmore & Goldreich (1984) define the mass within a distance  $r$  from the symmetry center by  $m(r, t) = \int_0^r x^{n-1} \rho(x, t) dx$ , where  $n = 1, 2$ , and  $3$  refer, respectively, to planar, cylindrical, and spherical perturbations. The mass within a fixed shell varies with time like  $m \sim t^{-2(3-n)/3}$ , because of the Hubble expansion along  $3 - n$  of the axes. In this notation, the equations of motion are, the continuity equation,

$$\frac{d(\rho t^{\frac{2(3-n)}{3}})}{dt} = -t^{\frac{2(3-n)}{3}} \rho r^{1-n} \partial_r (r^{n-1} v), \quad (1)$$

Euler,

$$\frac{dv}{dt} - \frac{2}{9} \frac{3-n}{n} \frac{r}{t^2} = -\frac{\partial_r p}{\rho} - \frac{4\pi G m}{r^{n-1}}, \quad (2)$$

adiabatic condition,

$$\frac{d}{dt} (p \rho^{-\gamma}) = 0, \quad (3)$$

and the relation,

$$\partial_r m = r^{n-1} \rho. \quad (4)$$

These equations are satisfied everywhere except at the shock where the fluid variables are described by jump conditions obtained from mass, momentum, and energy conservation. The initial conditions leading to self-similar collapse are specified at an early time close

to zero,  $t_i$ , as

$$\frac{\delta M}{M} = \left(\frac{r}{r_0}\right)^{-s}, \quad (5)$$

$$v(r, t_i) = \frac{2}{3t_i} r, \quad (6)$$

$$p(r, t_i) = 0, \quad (7)$$

where  $\delta M/M$  is the mean density contrast interior to  $r$ , and  $s > 0$ . For cosmological initial conditions the initial density contrast must be tiny, so we will be interested in the solution in the region  $r \gg r_0$ . A perturbation with  $s > n$  can be realized by placing a high narrow positive density peak at the center ( $\ll r_0$ ) of a symmetric void with local density contrast  $\sim (-r^{-s})$ . The condition (6) means that a gas shell at  $r$  moves initially with the general universal expansion. This condition can be relaxed to allow for a non vanishing initial zero peculiar velocity according to late time linear theory (e.g., Peebles 1980). However, this does not affect the details of the collapse (Peebles 1980, Bertschinger 1985), so we use (6) which is commonly adopted in the literature. Bertschinger (1985) and White & Forcada (1997), respectively, considered the collapse of spherical perturbations with  $s = 3$ , and  $s = 2$ .

The equations of motion (1–4) together with the initial conditions (5–7) are insufficient to completely determine the evolution of the perturbation. Still missing is an inner boundary condition specifying the velocity and mass at  $r = 0$ , for  $t \geq t_i$ . For a shock to develop without the accumulation of a central mass (a black hole for  $n = 3$ ) we must have  $v(r = 0, t \geq t_i) = 0$  and  $m(r = 0, t \geq t_i) = 0$ . Relaxing the condition  $V(0) = 0$  leads to a non-vanishing central mass with or without the presence of a shock.

In a critical density universe ( $\Omega = 1$ ) the only length scale relevant to the collapse is the scale of non-linearity. At any time,  $t$ , this scale can be defined as the distance of the shell at the maximum expansion, i.e., the shell with  $v = 0$  (Gunn 1977, Fillmore & Goldreich 1984, Bertschinger 1985). This radius is termed the current turnaround radius,  $r_{ta}(t)$ . Starting from tiny initial density contrast, the mean overdensity (density in units

of  $\rho_c$ ) interior to  $r_{ta}(t)$  is a fixed number independent of time. For time  $t \gg t_i$ , when shells with  $r \gg r_0$  reach their turnaround, the collapse develops a self-similar behaviour that depends on  $r$  and  $t$  through the combination  $\lambda = r/r_{ta}$ . The turnaround radius  $r_{ta}(t)$  is given by (e.g., Fillmore & Goldreich 1984),

$$r_{ta} = r_0 \frac{C_x}{C_t^{3\alpha/2}} \left(\frac{t}{t_i}\right)^\alpha \quad ; \quad \alpha = \frac{2s+1}{3s} \quad (8)$$

where,

$$C_x = \frac{5}{12}, 0.741, 1 \quad ; \quad C_t = \frac{5}{6}, 1.386, \left(\frac{3\pi}{4}\right)^{2/3}, \quad (9)$$

for  $n = 1, 2$ , and  $3$ , respectively. The turnaround radius grows faster than the scale factor  $a \sim t^{2/3}$ . This is because the mass,  $\sim \rho_c r_{ta}(t)^3$ , interior to  $r_{ta}$  must grow with time while the mass,  $\sim \rho_c a^3(t)$ , inside a fixed shell in a homogeneous universe is constant. For  $s < 2$  the turnaround radius grows faster than  $t$  reaching the horizon scale in finite time. When this happens relativistic description must be used and  $r_{ta}$  ceases to be the only scale in the problem (Fillmore & Goldreich 1984).

The equations can be cast into a non-dimensional form using the scaled variables  $V(\lambda)$ ,  $D(\lambda)$ ,  $P(\lambda)$ , and  $M(\lambda)$  defined by (Bertschinger 1985),

$$v(r, t) = \frac{r_{ta}}{t} V(\lambda) \quad (10)$$

$$\rho(r, t) = \rho_c D(\lambda) \quad (11)$$

$$p(r, t) = \rho_c \left(\frac{r_{ta}}{t}\right)^2 P(\lambda) \quad (12)$$

$$m(r, t) = \frac{1}{3} \rho_c r_{ta}^n M(\lambda) . \quad (13)$$

Expressed in terms of these variables, the equations (1-4) become, respectively,

$$(V - \alpha\lambda) D' + \left(\frac{n-1}{\lambda} V + V' - \frac{2n}{3}\right) D = 0 , \quad (14)$$

$$(\alpha - 1) V + (V - \alpha\lambda) V' - \frac{2}{9} \frac{3-n}{n} \lambda = -\frac{P'}{D} - \frac{2}{9} \frac{M}{\lambda^{n-1}} , \quad (15)$$

$$\left(\gamma \frac{D'}{D} - \frac{P'}{P}\right) (V - \alpha\lambda) = 2(\alpha - 2 + \gamma) , \quad (16)$$

$$M' = 3\lambda^{n-1} D , \quad (17)$$

where the prime symbol denotes derivatives with respect to  $\lambda$ .

We will mainly be concerned with solutions for shocked collapse with vanishing mass at the center. The inner boundary condition appropriate for this collapse are vanishing mass and velocity at  $\lambda = 0$ , i.e.,

$$V(0) = 0 \quad \text{and} \quad M(0) = 0 , \quad (18)$$

Self-similarity implies that the shock appears at fixed  $\lambda = \lambda_s = r_s/r_{ta}$ , so the physical radius of the shock  $r_s \propto t^\alpha$  and its non-dimensional speed is  $(r_{ta}/t)^{-1} (dr_s/dt) = \alpha\lambda_s$ . At the surface of the shock the fluid variables satisfy the jump conditions obtained from mass, momentum, and energy conservation. In terms of the non-dimensional fluid variables, the jump conditions appropriate for an adiabatic shock are,

$$V^+ = \alpha\lambda_s + \frac{\gamma-1}{\gamma+1} (V^- - \alpha\lambda_s) , \quad (19)$$

$$D^+ = \frac{\gamma+1}{\gamma-1} D^- , \quad (20)$$

$$P^+ = \frac{2}{\gamma+1} D^- (V^- - \alpha\lambda_s)^2 , \quad (21)$$

$$M^+ = M^- , \quad (22)$$

where the superscripts of the minus and plus signs refer to pre- and post-shock quantities. In employing energy conservation we have taken  $\frac{P}{D(\gamma-1)}$  as the non-dimensional internal energy per unit mass.

In section 4 we will find numerical solutions satisfying the requirements for shocked collapse without a central mass. Except spherical perturbations with  $\gamma = 4/3$  only one value  $\lambda_s$  can yield solutions satisfying these requirements. Spherical perturbations with  $\gamma = 4/3$  allow a range of values for  $\lambda_s$ . Before presenting the numerical solutions we derive in the next section the asymptotic behaviour of the fluid variables near the center, and two integrals of motion which will be used as a check on the numerical solutions.

### 3 INTEGRALS OF MOTION AND ASYMPTOTIC BEHAVIOUR NEAR THE CENTER

Solutions to (14–17) with the appropriate jump and boundary conditions for all  $\lambda$  will be found by numerical integration. We present here an analytic treatment of the equations to derive the asymptotic behaviour of the fluid variables near  $r = 0$ , and two integrals of motion (e.g., Bertschinger 1983, 1985). We restrict the analysis shocked collapses satisfying the inner boundary condition (18). All fluid variables can be expressed in terms of an auxiliary function  $K(\lambda) \equiv \exp \int_0^\lambda \frac{dx}{V(x) - \alpha x}$  as follows.

$$V(\lambda) = \frac{K}{K'} + \alpha\lambda, \quad (23)$$

$$\frac{D(\lambda)}{D_0} = -\lambda^{1-n} K' K^{-1+n(2/3-\alpha)}, \quad (24)$$

$$\frac{P(\lambda)}{P_0} = -\lambda^{(1-n)\gamma} K^{4+(2n/3-3)\gamma-\alpha(2+n\gamma)} K'^{\gamma}, \quad (25)$$

$$\frac{M(\lambda)}{D_0} = \frac{9K^{n(2/3-\alpha)}}{n(3\alpha-2)}, \quad (26)$$

where  $D_0$  and  $P_0$  are constants. The fluid variables in (23–26) satisfy the non-dimensional equations (14), (16), and (17) for any functional form of  $K$ . The function  $K$  is then specified by only one equation, the non-dimensional Euler equation (15).

Two integrals of motion can immediately be found from (23–26). These are the mass and entropy integrals of motion (Bertschinger 1983, 1985),

$$M = \frac{9}{n(2-3\alpha)} D(V - \alpha\lambda) \lambda^{n-1}, \quad (27)$$

$$PD^{-\gamma} M^\zeta = \text{const} \quad ; \quad \zeta = \frac{6}{n} \frac{\alpha + \gamma - 2}{2 - 3\alpha}, \quad (28)$$

where all fluid variable are evaluated at any  $\lambda$  inside the shock. Since  $\zeta < 0$ , the entropy integral of motion means that the entropy  $\propto \ln(PD^{-\gamma})$  is an increasing function of the mass and hence  $\lambda$ .

The auxiliary function greatly simplifies the derivation of the asymptotic behaviour of the non-dimensional fluid variables near  $\lambda = 0$ . Since  $V(0) = 0$  and  $M(0) = 0$ , equations (23) and (26) imply that, to first order,  $K(\lambda)$  must approach

$$K(\lambda) = \lambda^{1/(V_0-\alpha)} \quad (29)$$

as  $\lambda \rightarrow 0$ , where  $V_0$  is an arbitrary constant. Substituting this expression for  $K$  in (23–26), yields

$$V = V_0\lambda, \quad (30)$$

$$M = \frac{9D_0}{n(3\alpha-2)} \lambda^{\delta+n}, \quad (31)$$

$$D = \frac{D_0}{\alpha - V_0} \lambda^\delta, \quad (32)$$

$$P = \frac{P_0}{(\alpha - V_0)^\gamma} \lambda^\eta, \quad (33)$$

and the asymptotic exponents are expressed in terms of the coefficient  $V_0$  as

$$\delta = \frac{n(2-3V_0)}{3(V_0-\alpha)}, \quad (34)$$

$$\eta = \frac{4-2\alpha-2\gamma+(\frac{2}{3}-V_0)n\gamma}{V_0-\alpha}. \quad (35)$$

These relations have been obtained without using the Euler equation (15). In order to determine the exponents uniquely we use the Euler equation which adds the following constraints,

$$\eta = 2(\delta + 1), \text{ for } \eta < 0,$$

$$2(\delta + 1) \geq 0, \text{ for } \eta = 0. \quad (36)$$

A value  $\eta > 0$  gives  $P_0 < 0$  and so, by (28), a negative entropy integral of motion. But the jump condition (21) gives positive pressure,  $P^+$ , just behind the shock and since the density and mass are also positive, the entropy integral (28) must be positive. So we rule out  $\eta > 0$ .

If the solution to (34), (35), and (36) is  $\eta < 0$  then the Euler equation also provides the following constraint on the coefficients  $P_0$  and  $D_0$ ,

$$P_0 = \frac{2D_0^2\alpha(V_0-\alpha)^{\gamma-1}}{n\eta(3\alpha-2)}. \quad (37)$$

Table 1 lists the values of  $V_0$ ,  $\eta$ , and  $\delta$  in all cases. The dashed curves in figure 1 are a graphical representation of the density exponent  $\delta$  versus  $s$  for  $\gamma = 5/3$ . In planar geometry,  $n = 1$ , the only possible solution to equations is  $\eta = 0$  and the pressure is finite everywhere. In cylindrical geometry,  $n = 2$ , we have  $\eta < 0$  only for  $\alpha < \frac{5\gamma-6}{3(\gamma-1)}$ , so it must be zero for other values of  $\alpha$ . In spherical geometry,  $n = 3$ , if  $\alpha < 2$  and  $\gamma > 4/3$  then  $\eta = 2(1 - \frac{2}{\alpha})$ , and  $V_0 = 0$  meaning that  $V(\lambda) \propto \lambda^\nu$ ,

where  $\nu > 1$ . A second order expansion gives  $\nu = 1 + 2\alpha^{-1} \left[ (4 - 5\alpha) \pm \gamma^{-1/2} \sqrt{8\alpha(\gamma - 8) + 16\gamma + \alpha^2(32 + \gamma)} \right]$ , where only one of the roots is  $\nu > 1$ . In the limit of either  $\alpha \rightarrow 2$  or  $\gamma \rightarrow 4/3$ , we have  $\nu \rightarrow 1$ .

For  $n = 3$  and  $\gamma = 4/3$  the relations (34), (35), and (36) allow multiple solutions for  $V_0$  and consequently for  $\lambda_s$ . A second order calculation gives the upper limit  $V_0 < 4 - 5\alpha$ . Solutions exist for any positive  $\lambda_s$  smaller than a maximal value which corresponds to the upper limit on  $V_0$ . This means that for  $\gamma = 4/3$  a shocked collapse cannot be accompanied by the presence of a non-vanishing mass at the center. In the table we list the asymptotic constants corresponding to  $V_0 = 4 - 5\alpha$ , i.e., the maximal value of  $\lambda_s$  for which a shocked collapse occurs. Bertschinger (1984) does not mention that there are solutions for shocked without a central mass for a range of  $\lambda_s$ . His numerical solution with  $\gamma = 4/3$  seems to correspond to the maximal  $\lambda_s$  and yields  $\eta = -3.2$  and  $\delta = -2.6$ , instead of  $-3$  and  $-2.5$  as listed in table 1.

We now examine how the dimensional density,  $\rho(r, t) = \rho_c D$ , varies with time near the center. Using  $\rho_c \sim t^{-2}$ , the first order expression  $D \sim (r/r_{ta})^\delta$ , and  $r_{ta} \sim t^\alpha$ , we find  $\rho(r, t) \sim r^\delta / t^{2+\alpha\delta}$ . When  $2 + \delta\alpha = 0$  the density is constant with time. In spherical geometry a time independent density is equivalent to  $V_0 = 0$ . Because of the expansion in the  $n - 1$  directions, a vanishing  $V_0$  in planar and cylindrical geometries leads to  $\rho \sim t^{-2-\alpha\delta} \sim t^{2(n-1)/3}$ . In all geometries a vanishing  $V_0$  indicates that, to first order in the asymptotic expansion, the gas is pressure supported in hydrostatic equilibrium. According to the table, spherical perturbations have  $V_0 = 0$  only for  $s > 1/2$ . Note that for  $2 > s > 1/2$  the asymptotic density is constant even though the temperature  $\sim P/D \sim r^{\eta-\delta}$  decreases inward. For  $s < 1/2$ , the density increases with time. According to table 1, planar and cylindrical perturbations have  $V_0 = 0$  only at  $s = 1/(2 - \gamma)$  and  $s = 2/(4 - \gamma)$ , respectively.

#### 4 NUMERICAL INTEGRATION

We present results of the numerical integration of the non-dimensional equations of motion. The numerical solutions shown here describe shocked collapses without a central mass. Outside the shock the fluid variables are given from the solution for collapse with zero pressure (Zel'dovich 1970, Peebles 1980, Fillmore & Goldreich 1984).

The shock position  $\lambda_s$  is unknown a priori. We have to find its value such that the fluid variables satisfy the equations of motion, (14–17), the jump conditions, (19–22), and the inner boundary condition, (18). Assuming that the pre-shock variables are given from the zero pressure solution, the value of  $\lambda_s$  can be found as follows (Bertschinger 1985, Forcada–Miro & White 1997). For an assumed value for  $\lambda_s$ , we obtain the post-shock variables using the jump conditions. We then integrate the equations of motion from  $\lambda_s$  inward to  $\lambda = 0$ , and tune  $\lambda_s$  so that the solution gives  $V = 0$  and  $M = 0$  at  $\lambda = 0$ . In all numerical solutions we find that if  $M(0) = 0$  for a given  $\lambda_s$  then  $V(0) = 0$ , and vice versa.

The zero pressure solutions in planar and spherical geometries are known analytically (Zel'dovich 1970, Fillmore & Goldreich 1984) so the pre-shock fluid variable can be found directly, for an assumed  $\lambda_s$ . However in cylindrical geometry an analytic solution is not available and we numerically integrate the equations with zero pressure to obtain the pre-shock quantities. In practice we use numerical integration also in planar and spherical geometries. It is convenient to integrate the zero pressure equations from  $\lambda = 1$ , i.e., the turnaround radius, to  $\lambda_s$ . At  $\lambda = 1$  the fluid variables are

$$V(1) = 0 \quad , \quad P(1) = 0 \quad , \quad (38)$$

$$D(1) = \frac{1}{s+1} \left( \frac{C_t}{C_x} \right)^n \quad , \quad M(1) = \frac{3}{n} \left( \frac{C_t}{C_x} \right)^n \quad , \quad (39)$$

where the expressions for  $D(1)$  and  $M(1)$  were obtained from the zero pressure solution (e.g., Fillmore & Goldreich 1984).

The sequence of figures (2–5) shows the numerical solutions for the over density  $D$ , the pressure  $P$ , the velocity  $V$ , and the thermal energy  $U = \frac{P}{D(\gamma-1)}$  in spherical, cylindrical and planar geometries for several values of  $s$ , all as a function of  $\lambda$ . All curves are obtained from the solutions with  $\gamma = 5/3$ . The solid curve in each plot corresponds to  $s = n$ . The sudden change in the fluid variables indicate the location of the shock. All numerical solutions satisfy the integrals of motion (27) and (28) up to the numerical accuracy and agree with asymptotic behaviour of the previous section. The logarithmic slopes of all curves match the corresponding values listed in table 1. Spherical perturbations with  $s = 3$  and  $s = 2$  were, respectively, analyzed by Bertschinger (1984) and Forcada–Miro & White (1997). The agreement between their solutions with  $\gamma = 5/3$  and ours is excellent. In all geometries the density and pressure in the shock are higher for larger  $s$ . Figures 4 of the velocity and figure 5 of the internal energy  $U = \frac{P}{D(\gamma-1)}$  demonstrate that particles are decelerated at the shock converting most of their kinetic energy into heat. The velocity near the center of cylindrical perturbations can be positive inside the shock, hence the linear vertical scale in velocity plot in this case.

In figure 6 we plot the location of the shock  $\lambda_s$  as a function of  $s$  for several values of  $\gamma$ . The shock location always increases with  $s$  and agrees with the values obtained by Bertschinger (1985) and Forcada–Miro & White (1997) for spherical perturbations with  $s = 3$  and  $s = 2$ , respectively. A special case is spherical collapse with  $\gamma = 4/3$ . Here a solution for shocked collapse without a central point mass is possible for any  $\lambda_s$  less than a maximal value  $\lambda_c$ . In this case we plot the maximal value  $\lambda_c$ . For  $s \gg 1$ ,  $\lambda_s$  can exceed unity increasing to a finite value as  $s \rightarrow \infty$ .

The variation of the fluid variables attached to a given fluid elements are also of interest. Using the velocity obtained from the self-similar solutions we can calculate the trajectory  $r(t)$  of a fluid element (particle) as a function of time. The fluid variable associated with the particle at any time can then be obtained by

interpolating the solutions at the particle’s position at that time. The three panels from top to bottom in figure 7 show, respectively, the trajectory, density, and pressure of a particle as obtained from the solutions with  $\gamma = 5/3$  for three values of  $s$ . The time axis in all panels is  $t/t_{ta}$  where  $t_{ta}$  is the time at which the particle reached its maximum expansion (the turnaround time). The particle position,  $r$ , density  $\rho$ , have been scaled by their values at  $t_{ta}$ ,  $r'_{ta} = r(t_{ta})$ , and  $\rho = \rho(t_{ta})$ , respectively. The pressure,  $p$ , has been scaled by its value at the shock  $p_s$ . With this scaling the curves in the figures become valid for all the particles. The particle trajectory for  $s = 3$  (solid line, top panel) agrees with the corresponding curve in figure 4 of Bertschinger (1985). As expected from the asymptotic solution the particles for  $s = 3$  and  $s = 10$  tend to settle at a physical distance which is a fixed fraction of their turnaround radii. The decay of the trajectory for  $s = 1/4$  at late time can be evaluated using the asymptotic expansion. Near the origin  $V(\lambda) = V_0\lambda$ , so  $dr/dt = (r_{ta}/t)V_0\lambda = -r/t$  and  $r \sim t^{V_0}$ . According to table 1  $V_0 = -8/15$  for  $s = 1/4$  and  $\gamma = 5/3$  so  $r$  decays like  $t^{-8/15}$ . The density (middle panel) and pressure (bottom) curves for  $s = 3$  and  $s = 10$  flatten at late times, consistent with the settling of the particles to a constant  $r$ .

## 5 ASYMPTOTIC BEHAVIOUR IN A UNIVERSE DOMINATED BY COLLISIONLESS MATTER

So far we have considered similarity solutions for collapse involving gas only. The collapse of scale free symmetric perturbations in an Einstein–De Sitter universe containing a mixture of gas and collisionless matter is also self-similar. Similarity solutions for mixed collapse are beyond the scope of the present paper. Here we only obtain the asymptotic behaviour of the gas variables in a universe dominated by collisionless matter. For a self-similar collapse to develop, the two matter components must start with the same initial conditions with zero initial gas pressure. Shells of gas and collisional matter

then move together until they reach either a shock in the gas or the region of shell crossing in the collisionless component. The evolved density profiles of both components depend on  $r$  and  $t$  through  $\lambda$ . Although the global gas mass fraction is negligible, the gas can be gravitationally dominant at the center of the collapse if it has a steeper density profile than the collisionless matter. For the purpose of deriving the asymptotic exponents we proceed assuming that the gravity of the gas is negligible everywhere and check the consistency of this assumption according to the results. So we replace the gas mass  $M(\lambda)$  in the non-dimensional Euler equation (15) by the collisionless matter mass  $\tilde{M}(\lambda)$ . Writing  $\tilde{M} \sim \lambda^{\tilde{\delta}+n}$  near  $\lambda = 0$ , Fillmore & Goldreich (1984) find that  $\tilde{\delta}$  is

$$n = 1: \quad \tilde{\delta} = \frac{-s}{s+1} \quad (40)$$

$$n = 2: \quad \tilde{\delta} = -1 \quad (41)$$

$$n = 3: \quad \begin{aligned} \tilde{\delta} &= -2, \quad \text{for } s \leq 2 \\ &= \frac{-3s}{s+1}, \quad \text{for } s > 2 \end{aligned} \quad (42)$$

Table 2 summarizes the values of the asymptotic constants obtained by substituting the asymptotic behaviour of the collisionless mass in the non-dimensional Euler equation. The dotted and dashed curves in figure 1 represent the density exponent vs  $s$  computed from table 1 and table 2, respectively, for  $\gamma = 5/3$ . The solid curve is the collisionless matter exponent  $\tilde{\delta}$  versus  $s$ .

In spherical perturbations we see from the tables and figure 1 that the asymptotic gas density profile in a universe with collisionless matter is steeper than that containing gas only. For  $s > 2$  the density asymptotic exponents of the gas and collisionless matter are identical. For  $s < 2$  the collisionless matter density profile is steeper. This is consistent with neglecting the gravity of the gas near the center. As  $\gamma \rightarrow 4/3$  gas density exponent approaches  $-2$  for  $s < 2$  and  $-3s/(1+s)$  otherwise, so the gas has the same asymptotic profile as the collisionless matter for all  $s$ .

In cylindrical perturbations with  $s$  large enough, the gas has a steeper density profile than the collisionless matter. This means that virial motions in the collisionless matter are more effective at balancing gravity than the gas pressure force. So for large  $s$  the derivation of the asymptotic exponent in section 3 is more suitable. A steeper gas profile also occurs in planar perturbations with  $s < 1/(3-\gamma)$ . However the asymptotic constants obtained here and in section 3 are identical in planar geometry.

In spherical perturbations with  $s > 2$ , the density  $\rho(r, t)$  is constant with time and the temperature  $\sim p/\rho$  diverges like  $r^{\frac{2-s}{1+s}}$  as  $r \rightarrow 0$ . To first order in the asymptotic expansion where the gas can be in hydrostatic equilibrium in the dominant potential well of the collisionless matter. For  $s < 2$  the density increases with time and the temperature is constant near the center. For comparison, in the absence of collisionless matter, for  $2 > s > 1/2$  the temperature decreases inward but the gas is in hydrostatic equilibrium to first order in the asymptotic expansion.

## 6 DISCUSSION

The similarity solutions are found for collapse in a flat universe with matter density parameter  $\Omega = 1$ . Because of Birkhoff's theorem, the solutions for spherical collapse are valid in an open universe if the current turnaround radius is well inside the spherical region interior to which the perturbation is bound. The statement is incorrect for planar and cylindrical perturbations because of the explicit appearance of cosmology dependent terms in the equations of motion (1–4), like  $t^{2(3-n)/3}$  in the continuity equation (1).

The solutions are appropriate for the adiabatic collapse of perturbations with deep gravitational potential so that the initial thermal energy of the gas can be ignored. Such perturbations are probably the seeds for massive galaxies, galaxy groups and clusters. In the intergalactic medium (IGM) most of the gas is continu-

ously photo-heated and is of moderate density. There is considerable interest in analytic modelling of the IGM in current methods for extracting cosmological information from the Lyman forest (Croft et. al. 1998, Nusser & Haehnelt 1999, 2000). So far these methods have heavily relied on linear analysis (e.g., Bi, Börner, & Chu 1992, Gnedin & Hui 1998, Nusser 2000) and hydrodynamical simulations (e.g., Petitjean et. al. 1995, Theuns et. al. 1999). Analytic treatment of the IGM beyond the linear regime is exceedingly complicated. Consider a situation in which photo-heating establishes the relation  $p = k\rho^\gamma$  in the IGM, where  $k$  and  $\gamma$  depend non-trivially on time (e.g., Theuns et. al. 1999). The pressure in this case introduces a length scale  $k^{1/2}G^{(1-\gamma)/2}t^{2-\gamma}$  (e.g., Sedov 1959). If we take constant  $k$  and  $\gamma$ , this length scale varies with time like  $r_{ta}$  only in the special case of  $\gamma = 4/3$  and infinite  $s$ . So physically interesting situations including initial pressure in which the collapse is self-similar do not exist.

Spherical Perturbations with  $s > 2$  when  $\gamma > 4/3$ , and with any  $s > 0$  when  $\gamma = 4/3$  deserve special attention. In the corresponding solutions for shocked collapse without a black hole at the center, the quantity  $V_c^2 = 2Gm/r$  diverges towards the center, and so there is a point  $r = r_g$  at which  $V_c^2 = c^2$ , where  $c$  is the speed of light. According to general relativity this implies the presence of a black hole at the center, invalidating the assumption of no central mass, made in deriving the solutions. In particular, the condition  $v(r = 0) = 0$ , necessary for shocked collapse, is incompatible with the presence of a central black hole. Near  $r_g$ , however, radiation pressure and angular momentum can prevent the formation of a black hole. Should this occur, we expect our solution for shocked accretion to be valid away from the central region.

The evolved gas variables in the symmetric self-similar collapse contain full information on the initial perturbation. So the system retains memory of the initial conditions, even in the highly nonlinear regime. On the other hand, a collapsing system of collisionless matter can develop density profiles which do not depend on

the initial shape of the perturbation. For example, according to the solutions of Fillmore & Goldreich (1984), a spherical density perturbation develops into  $r^{-2}$  for  $s < 2$ , and a cylindrical perturbation into  $r^{-1}$  for all  $s$ . Haloes identified in cosmological simulations of collisionless particles with generic initial conditions, also tend to have density profiles independent of the spectrum of the initial fluctuations (Navarro, Frenk & White 1997).

Our results are relevant for describing the gas distribution in various physical systems such as the cores of clusters or pancake-like superclusters. Over a limited range of scales, the index  $s$  can be related to the index,  $l$ , of the three dimensional power spectrum,  $p(k) \sim k^l$ , of the linear density fluctuations. If the initial density field is gaussian with a scale free power spectrum then the properties of the nonlinear field depend only on one scale. This is the nonlinear scale,  $R_{nl}$ , defined as the scale on which the rms value of density fluctuations is unity. This scale grows with time like  $R_{nl} \sim t^{\frac{2(l+5)}{3(l+3)}}$ . By matching the time dependence of  $R_{nl}$  and  $r_{ta} \sim t^{\frac{2(s+1)}{3s}}$  we identify  $s = (l + 3)/2$ . So the collapse of gas into galaxies and clusters can be, respectively, modeled by our solutions for  $s \sim 0.4$  and  $0.65$ , where we have taken  $l \sim -2.2$  and  $-1.7$  assuming a Cold Dark Matter power spectrum. Taking  $l \sim -1$  for collapse on a pancake-like large scale superclusters gives  $s \sim 1$ . Another way to relate  $s$  and  $l$  is to identify symmetric perturbations with local maxima in the linear density field (Hoffman & Shaham 1985). The shape of high density peaks in a gaussian field varies with  $r$  like the two-point correlation function,  $\sim r^{-(l+3)}$  (e.g., Bardeen et. al. 1986). So, at least in the limit of high peaks,  $s = l + 3$ . On galaxy and cluster scales the relation  $s = l + 3$ , respectively, gives  $s = 0.8$  and  $1.3$  in contrast to  $s = 0.4$  and  $0.65$  obtained from  $s = (l + 3)/2$ . Note however that gas in

\*  $R_{nl}$  does not involve the dimension  $n$  because  $l$  refers to the three dimensional  $p(k)$  so the rms value on a scale  $R$  is  $R^{(l+3)/2}$  independent of  $n$ .

galaxies tends to settle into disks and so our solutions are less relevant than they are for cluster size objects.

In spherical geometry the asymptotic behaviour shows that the gas cannot be pressure supported if  $s < 1/2$ , and  $s < 2$  for collapse with, and without collisionless matter, respectively. Estimates of the masses of rich galaxy clusters from X-ray observations of the intracluster gas rely on hydrostatic equilibrium (e.g., Fabian 1994). If on cluster scales  $s \sim 0.7\text{--}1.3$ , then the asymptotic behaviour implies that the cluster gas may not be in hydrostatic equilibrium. How large is the error introduced in the mass estimates by assuming hydrostatic equilibrium? The following argument shows that this error is negligible. Hydrostatic equilibrium calculations neglect the term  $G^{-1}r^2 dv/dt$  in the mass estimate. Using the asymptotic expansion one finds that neglecting this term amounts to a relative mass error of  $\sim (2/\pi^2)(t/t_{ta})^{3V_0-2}$  where  $t_{ta}$  is the turnaround time of the shell present at  $r$  at the current time  $t$ . Shells in the inner regions have passed their maximum expansion a few dynamical times ago. Therefore  $t \gg t_{ta}$  and since  $V_0 < 0$  we conclude that the error is negligible.

The solutions are related to modelling the structure of haloes made of self interacting dark matter (SIDM) (Spergel & Steinhardt 1999) with large interaction cross section. On scales of massive galaxies and clusters, our results predict final density profile  $\rho \sim r^{-1.2}$  to  $\sim r^{-1.7}$ . These profiles are consistent with the results obtained by Moore et. al. in their simulations of SIDM with large cross section.

## 7 ACKNOWLEDGEMENT

We thank the referee for useful comments. This research was supported by The Israel Science Foundation founded by The Israel Academy of Sciences and Humanities, and by the Fund for the Promotion of Research at The Technion.

## REFERENCES

- Bardeen J.M., Bond J.R., Kaiser N., Szalay A.S., 1986, ApJ, 304, 15
- Benson, A.,J., Cole, S., Frenk, C.S., Baugh, C.M., Lacey, C.G., 2000, MNRAS, 311, 793
- Bertschinger E., 1985, ApJS, 58, 39
- Bertschinger E., 1983, ApJ, 268, 17
- Bi H.G., Börner G., Chu Y., 1992, A&A, 266, 1
- Cole, S., Aragon-Salamanca, A., Frenk, C.S., Zepf, S.E., 1994, MNRAS, 271, 781
- Croft R.A.C., Weinberg D.H., Katz N., Hernquist L., 1998, ApJ, 495, 44
- Dekel A., Rees M.J., 1987, Nature, 326, 455
- Fabian A.C., 1994, Annu. Rev. Astron. Astrophys., 32, 277
- Fillmore J.A., Goldreich P., 1984, 281, 1
- Flores R.A., Primack J.R., ApJL, 427, 1
- Forcada-Miro M.I., White S.D.M., 1997, astro-ph/9712204
- Gnedin N., Hui L., 1998, MNRAS, 296, 44
- Gunn J.E., 1977, ApJ, 218, 592
- Hoffman Y., Shaham J., 1985, ApJ, 297, 16
- Kauffmann, G., Nusser, A., Steinmetz, M., 1997, MNRAS, 286, 795
- Kauffmann, G., White, S.D.M., Guiderdoni, B., 1993, MNRAS, 264, 201
- Moore B., Gelato S., Jenkins A., Pearce F.R., Quilis V., 2000, astro-ph/0002308
- Navarro J., Frenk C.S., White S.D.M., 1997, ApJ, 490, 493
- Nusser A., Haehnelt M., 1999, MNRAS, 303, 179
- Nusser A., Haehnelt M., 2000, MNRAS, 312, 364
- Nusser A., 2000, MNRAS, accepted
- Peebles P.J.E., 1980, *The Large Scale Structure in The Universe*, Princeton University Press, Princeton.
- Petitjean P., Mückel J.P., Kates R.E., 1995, A&A, 295, L9
- Sedov L., 1959, *Similarity and Dimensional Methods*, London: Cleaver-Hume press.
- Somerville, R.S., Primack, J.R., 1999, MNRAS, 310, 1087
- Spergel D.N., Steinhardt P/J., 1999, astro-ph/9909386
- Theuns T., Leonard A., Efstathiou G., Pearce F.R., Thomas P.A., 1998, MNRAS, 301, 478
- Zel'dovich Ya.B., 1970, Astron. & Astrophys., 5, 84

**Table 1.** Asymptotic constants,  $V_0$ ,  $\delta$ , and  $\eta$  for collapse of collisional gas only. Spherical perturbations with  $\gamma = 4/3$  allow a range of  $\lambda_s$ . Listed are the values corresponding to the maximal  $\lambda_s$ .

$n = 3, \gamma > 4/3$			
	$V_0$	$\eta$	$\delta$
$s \leq 1/2$	$\frac{4(2s-1)}{9s\gamma}$	0	$\frac{-3(2+s(3\gamma-4))}{2+3\gamma+s(3\gamma-4)}$
$s > 1/2$	0	$2\frac{1-2s}{s+1}$	$-\frac{3s}{s+1}$
$n = 3, \gamma = 4/3$			
	$\frac{2(s-5)}{3s}$	-3	-2.5
$n = 2, \gamma \geq 4/3$			
$s \leq \frac{2(\gamma-1)}{3\gamma-4}$	$\frac{s(4-\gamma)-2}{3s\gamma}$	0	$\frac{-2(2+s(3\gamma-4))}{2+2\gamma+s(3\gamma-4)}$
$s > \frac{2(\gamma-1)}{3\gamma-4}$	$\frac{2-\gamma}{3(\gamma-1)}$	$\frac{4(1-\gamma)+2s(3\gamma-4)}{2(1-\gamma)+s(4-3\gamma)}$	$\frac{2s(4-3\gamma)}{2(\gamma-1)+s(3\gamma-4)}$
$n = 1, \gamma \geq 4/3$			
	$\frac{-4(1+s(\gamma-2))}{3s\gamma}$	0	$\frac{s(4-3\gamma)-2}{2+\gamma+s(3\gamma-4)}$

**Table 2.** The gas asymptotic constants,  $V_0, \delta, \eta$  for mixed collapse with dominant collisionless matter.

$n = 3, \gamma \geq 4/3$			
	$V_0$	$\eta$	$\delta$
$s \leq 2$	$\frac{2(s-2)}{9s(\gamma-1)}$	$\frac{2+s(3\gamma-4)}{(1+4s)/3-\gamma(1+s)}$	$\frac{2+s(3\gamma-4)}{(1+4s)/3-\gamma(1+s)}$
$s > 2$	0	$2\frac{1-2s}{s+1}$	$-\frac{3s}{s+1}$
$n = 2, \gamma \geq 4/3$			
$s \leq \frac{2(\gamma-1)}{3\gamma-4}$	$\frac{s(4-\gamma)-2}{3s\gamma}$	0	$\frac{-2(2+s(3\gamma-4))}{2+2\gamma+s(3\gamma-4)}$
$s > \frac{2(\gamma-1)}{3\gamma-4}$	$\frac{2(1+s(\gamma-3))}{3s(1-2\gamma)}$	$\frac{2(\gamma-1)-s(3\gamma-4)}{2\gamma+s(3\gamma-4)}$	$\frac{-2+2s(4-3\gamma)}{2\gamma+s(3\gamma-4)}$
$n = 1, \gamma \geq 4/3$			
	$\frac{-4(1+s(\gamma-2))}{3s\gamma}$	0	$\frac{s(4-3\gamma)-2}{2+\gamma+s(3\gamma-4)}$

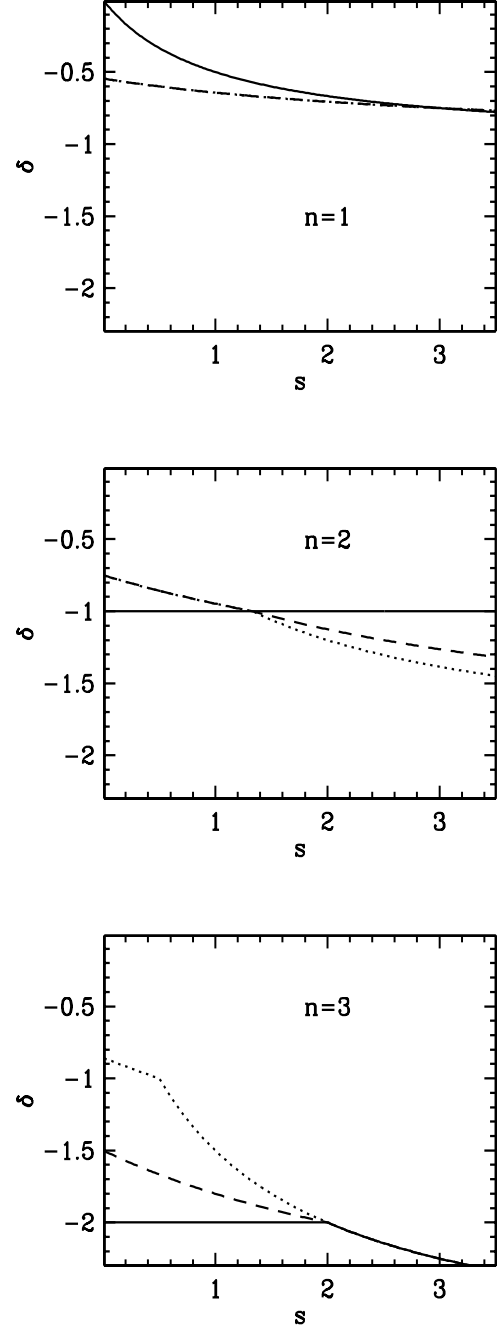


**Figure 1.** The density asymptotic exponent versus  $s$  for  $n = 1, 2$ , and  $3$ . The dashed and dotted curves are the gas exponent for collapse with and without collisionless matter, respectively. The curves are computed according to tables 1 and 2 with  $\gamma = 5/3$ . For  $n = 2$  the two curves overlap. The solid curve is the asymptotic exponent,  $\bar{\delta}$ , of the collisionless matter given by equations (40–42) (Fillmore & Goldreich 1984).

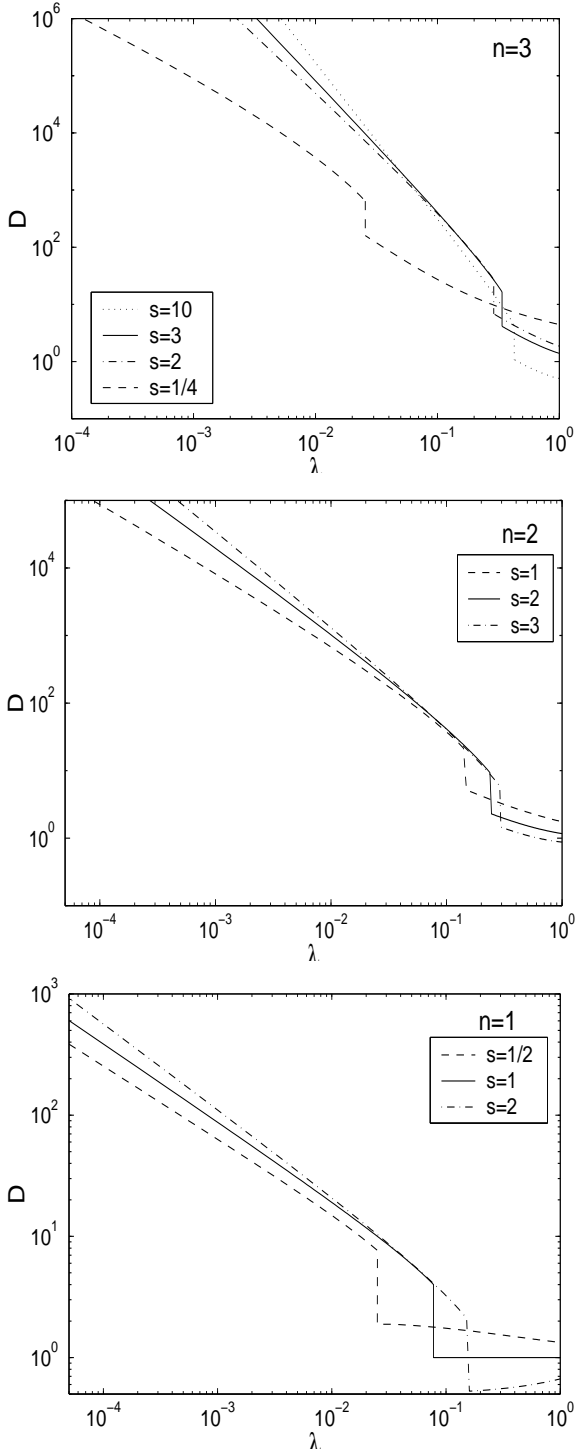


**Figure 2.** The over density  $D = \rho/\rho_c$  as a function of  $\lambda$  for various values of  $s$ . This and figures 3–5 show fluid variables obtained from numerical solutions with  $\gamma = \frac{5}{3}$ .

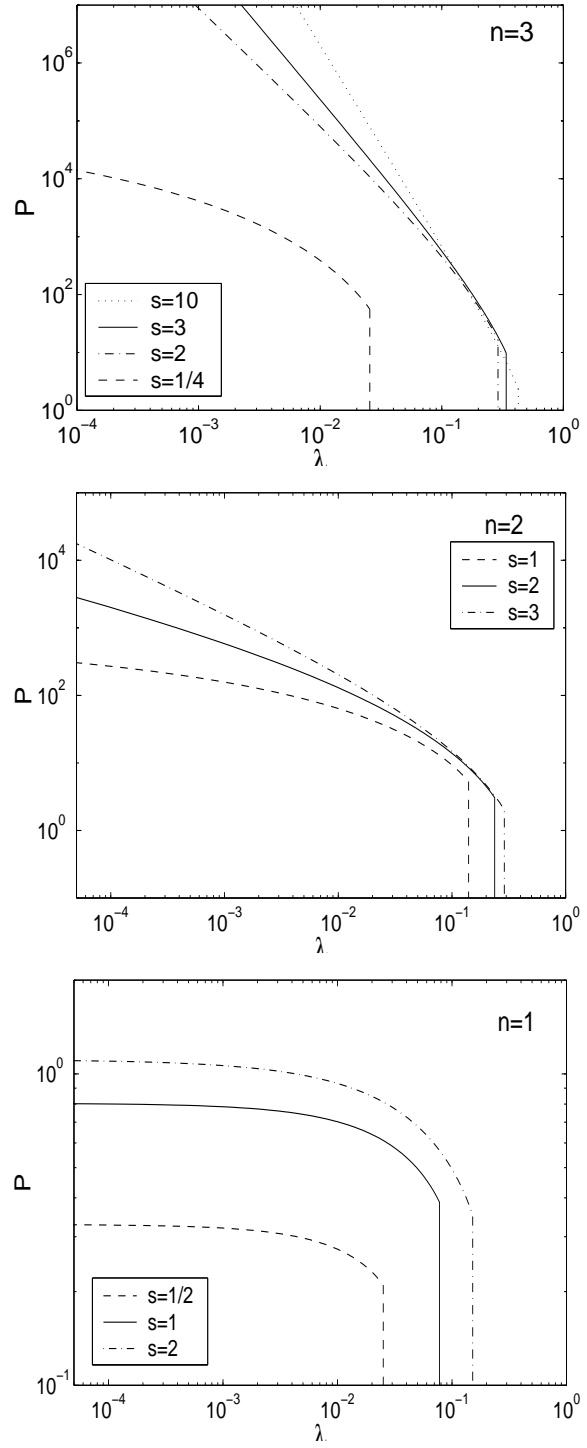


**Figure 3.** The pressure  $P$ .

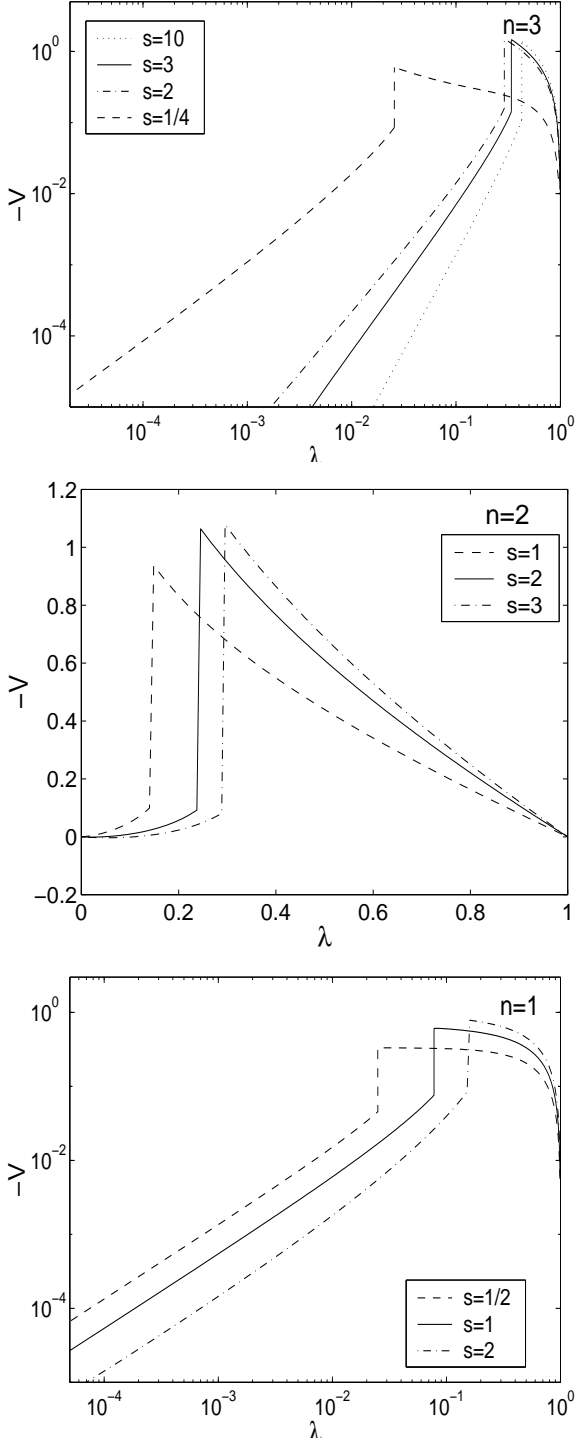


**Figure 4.** Curves of *minus* the velocity  $V$ . Linear vertical scale for  $n = 2$ .

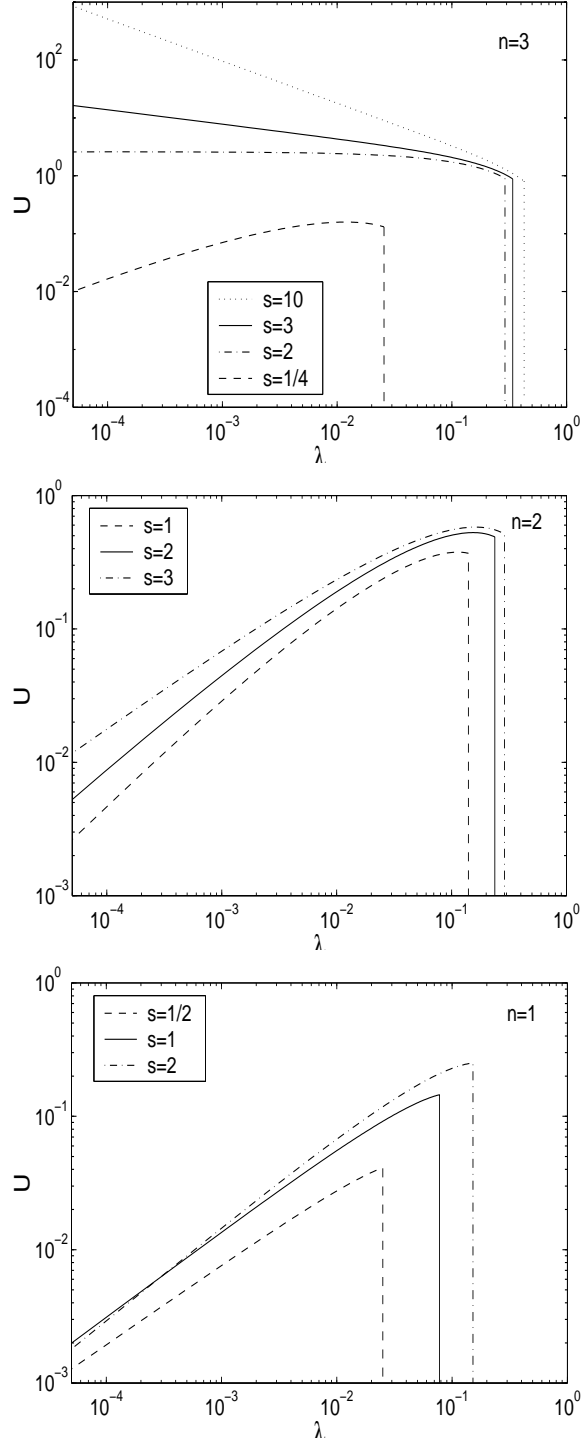


**Figure 5.** The thermal energy  $U = \frac{P}{D(\gamma-1)}$ .

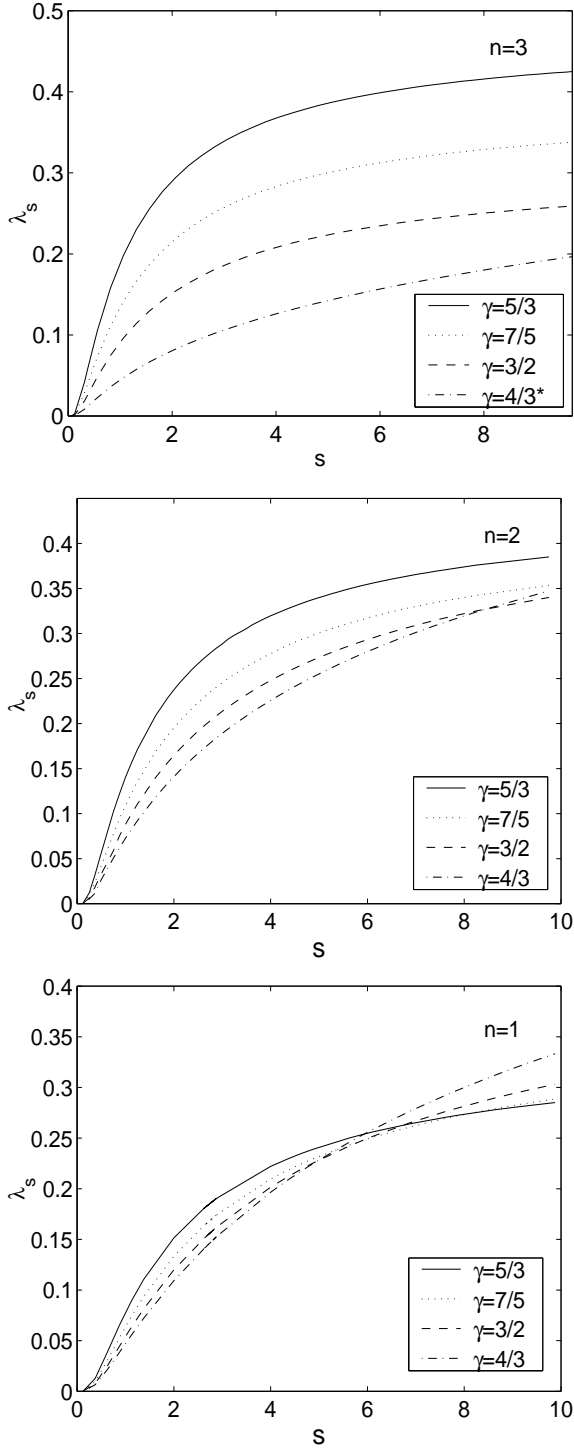


**Figure 6.** The shock location  $\lambda_s$  as a function of  $s$ .

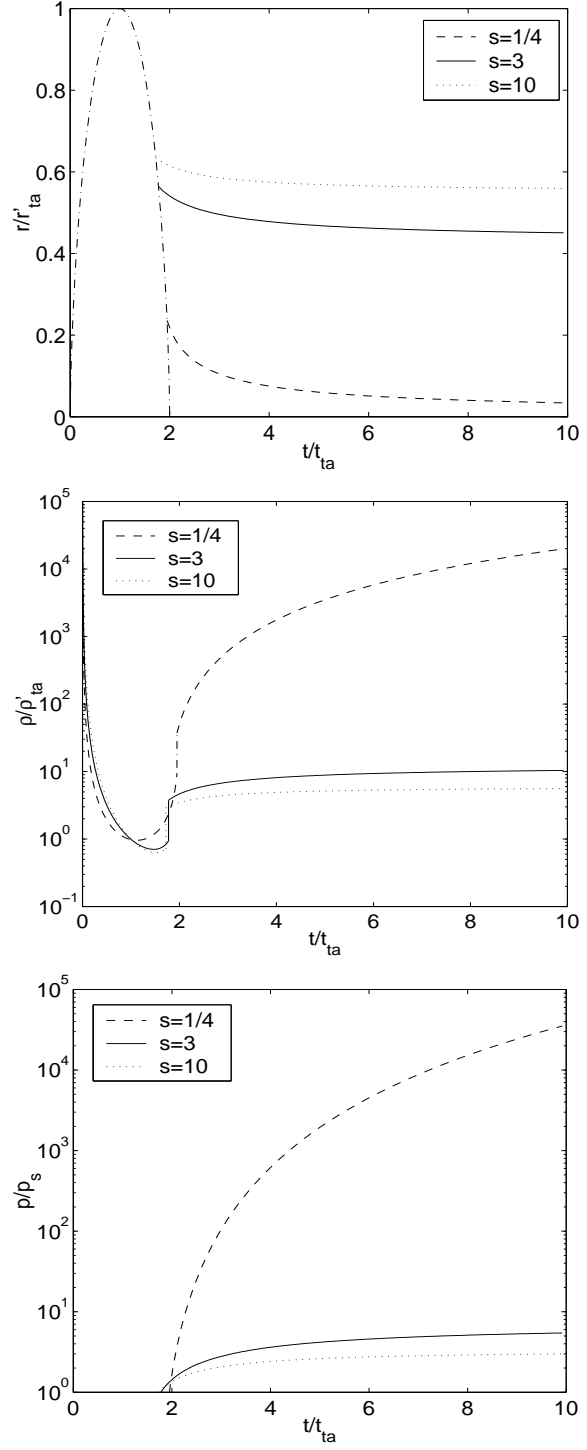


**Figure 7.** The trajectory and fluid variables of a particle as a function of time in spherical collapse with  $\gamma = 5/3$  for various  $s$ . The distance,  $r$ , and density,  $\rho$ , have been scaled by their respective values,  $r'_{ta}$ , and  $\rho'_{ta}$ , at the turnaround time  $t_{ta}$ , while the pressure,  $p$ , by its value,  $p_s$ , immediately after the particle crossed the shock.